

# Dosimetric impact of a robust optimization approach to mitigate effects from rotational uncertainty in prostate intensity-modulated brachytherapy

Björn Morén<sup>1</sup> | Majd Antaki<sup>2</sup> | Gabriel Famulari<sup>2,3</sup> | Marc Morcos<sup>2</sup> |  
Torbjörn Larsson<sup>1</sup> | Shirin A. Enger<sup>2,4</sup> | Åsa Carlsson Tedgren<sup>5,6,7</sup>

<sup>1</sup>Department of Mathematics, Linköping University, Linköping, Sweden

<sup>2</sup>Department of Oncology, Medical Physics Unit, McGill University, Montreal, QC, Canada

<sup>3</sup>Département de Radio-oncologie, Centre Hospitalier de l'Université de Montréal, Montreal, QC, Canada

<sup>4</sup>Lady Davis Institute for Medical Research, Jewish General Hospital, Montreal, QC, Canada

<sup>5</sup>Radiation Physics, Department of Health, Medicine and Caring Sciences, Linköping University, Linköping, Sweden

<sup>6</sup>Medical Radiation Physics and Nuclear Medicine, Karolinska University Hospital, Stockholm, Sweden

<sup>7</sup>Department of Oncology Pathology, Karolinska Institute, Stockholm, Sweden

## Correspondence

Björn Morén, Department of Mathematics, Linköping University, Linköping, Sweden.  
Email: [bjorn.moren@liu.se](mailto:bjorn.moren@liu.se)

## Funding information

Vetenskapsrådet, Grant/Award Number: VR-NT 2019-05416; Cancerfonden, Grant/Award Number: CAN 2017/1029; Canada Research Chairs, Grant/Award Number: 252135; Collaborative health research projects, Grant/Award Number: 523394-18

## Abstract

**Background:** Intensity-modulated brachytherapy (IMBT) is an emerging technology for cancer treatment, in which radiation sources are shielded to shape the dose distribution. The rotatable shields provide an additional degree of freedom, but also introduce an additional, directional, type of uncertainty, compared to conventional high-dose-rate brachytherapy (HDR BT).

**Purpose:** We propose and evaluate a robust optimization approach to mitigate the effects of rotational uncertainty in the shields with respect to planning criteria.

**Methods:** A previously suggested prototype for platinum-shielded prostate <sup>169</sup>Yb-based dynamic IMBT is considered. We study a retrospective patient data set (anatomical contours and catheter placement) from two clinics, consisting of six patients that had previously undergone conventional <sup>192</sup>Ir HDR BT treatment. The Monte Carlo-based treatment planning software RapidBrachyMCTPS is used for dose calculations. In our computational experiments, we investigate systematic rotational shield errors of  $\pm 10^\circ$  and  $\pm 20^\circ$ , and the same systematic error is applied to all dwell positions in each scenario. This gives us three scenarios, one nominal and two with errors. The robust optimization approach finds a compromise between the average and worst-case scenario outcomes.

**Results:** We compare dose plans obtained from standard models and their robust counterparts. With dwell times obtained from a linear penalty model (LPM), for  $10^\circ$  errors, the dose to urethra ( $D_{0.1cc}$ ) and rectum ( $D_{0.1cc}$  and  $D_{1cc}$ ) increase with up to 5% and 7%, respectively, in the worst-case scenario, while with the robust counterpart, the corresponding increases were 3% and 3%. For all patients and all evaluated criteria, the worst-case scenario outcome with the robust approach had lower deviation compared to the standard model, without compromising target coverage. We also evaluated shield errors up to  $20^\circ$  and while the deviations increased to a large extent with the standard models, the robust models were capable of handling even such large errors.

**Conclusions:** We conclude that robust optimization can be used to mitigate the effects from rotational uncertainty and to ensure the treatment plan quality of IMBT.

## KEYWORDS

high dose-rate brachytherapy, inverse treatment planning, prostate IMBT, robust optimization

Shirin A. Enger and Åsa Carlsson Tedgren contributed equally to this study

This is an open access article under the terms of the [Creative Commons Attribution-NonCommercial-NoDerivs](https://creativecommons.org/licenses/by-nc-nd/4.0/) License, which permits use and distribution in any medium, provided the original work is properly cited, the use is non-commercial and no modifications or adaptations are made.

© 2022 The Authors. *Medical Physics* published by Wiley Periodicals LLC on behalf of American Association of Physicists in Medicine.

## 1 | INTRODUCTION

Intensity-modulated brachytherapy (IMBT) was first proposed by Ebert,<sup>1</sup> and is a form of high-dose-rate brachytherapy (HDR BT) in which static or dynamic shields of high atomic number ( $Z$ ) are used to allow for an additional, directional, modulation of the dose distribution. While  $^{192}\text{Ir}$  is commonly used in conventional HDR BT, alternative isotopes have been proposed for IMBT, for example  $^{75}\text{Se}$ ,  $^{169}\text{Yb}$ , and  $^{153}\text{Gd}$ ,<sup>2–10</sup> which due to their lower photon energy are easier to shield.

In HDR BT, the radiation source is placed close to or within a tumor with catheters, needles, or applicators. Each catheter has a number of dwell positions from which the source can irradiate the surrounding tissue. In IMBT, shields that can rotate are housed within the catheters to reduce the radiation in various directions at each dwell position. Each combination of dwell position and shield angle is associated with a separate dwell time decision. The large number of such combinations significantly increases the degrees of freedom in the dose planning, compared to in conventional HDR BT.

The purpose of our study is to propose a dose planning approach that mitigates the possible adverse effects from rotational uncertainty. The IMBT technique is not yet used in clinical practice, but the awareness of dosimetric effects from uncertainty in the delivery equipment and the possibility to mitigate such effects are essential for assuring acceptance of the IMBT technique.

### 1.1 | Treatment aims

The general treatment aims for HDR BT are to irradiate the target with a high enough dose and to spare nearby organs at risk (OARs). For dose planning and evaluation purposes, the anatomical structures of interest are discretised into dose points, each corresponding to a small volume. Important evaluation criteria are derived from the dose–volume histogram (DVH), either as volume-at-dose or as dose-at-volume. The former, denoted  $V_x^s$ , describes the volume (or portion) of a structure  $s$  that receives at least a dose  $x$  Gray (Gy); the latter, denoted  $D_y^s$ , describes the smallest dose that is received in the  $y$  cc of structure  $s$  that receive the highest dose. The measures  $V_x^s$  and  $D_y^s$  are referred to as dosimetric indices (DIs). DIs are generally included in clinical treatment guidelines; see for example HDR BT guidelines for prostate cancer,<sup>11–13</sup> and for cervical cancer.<sup>14</sup>

The purpose of IMBT is to achieve a dose distribution, which is more conformal to the target than what is possible with conventional HDR BT. For prostate cancer, the aim can be to create a tunnel of reduced dose around the urethra, which passes through the target,

hence sparing the urethra while the target is still irradiated with a sufficiently high dose. There are promising results along this line, for example, by Famulari et al.,<sup>15</sup> in which the dose to urethra is reduced with on average 13%, and by Adams et al.,<sup>16</sup> in which the dose to urethra is reduced with between 29 and 44%, depending on the considered DI. A difference between these studies is the radiation source,  $^{169}\text{Yb}$ <sup>15</sup> and  $^{153}\text{Gd}$ ,<sup>16</sup> respectively.

For cervical cancer, an important planning aim is to deliver a nonsymmetric high-quality treatment by only activating dwell positions inside an intracavitary applicator without using a hybrid approach, which is a combination of interstitial needles and an intracavitary applicator. IMBT treatment with a rotating shield placed inside the tandem of an intracavitary applicator with  $^{192}\text{Ir}$  as the radiation source, has been shown<sup>17</sup> to provide dose plan quality comparable to conventional HDR BT with a hybrid approach. Further, the IMBT plan quality was significantly improved when replacing the  $^{192}\text{Ir}$  source with  $^{169}\text{Yb}$ .

### 1.2 | Optimization models for treatment planning

Mathematical models for dose planning of HDR BT were first based on linear penalties.<sup>18–21</sup> The linear penalty model (LPM) is a convex optimization problem, which is easy to solve, but a weakness of the model is that the aforementioned DI-based evaluation criteria from treatment guidelines are not explicitly included. Because of the importance of DIs in clinical guidelines, models with explicitly formulated DI constraints have later been proposed.<sup>22–28</sup> Such models are nonconvex and hence much harder to solve than the LPM. See the recent literature review<sup>29</sup> of optimization models for HDR BT and IMBT, and the recent review<sup>30</sup> of IMBT approaches.

Dose plan optimization for IMBT has commonly been based on quadratic penalty models (QPMs).<sup>31–34</sup> Such models are generally convex and thus considered easy to solve. However, a model with DIs has also been proposed for IMBT and conventional HDR BT.<sup>35</sup> In our study, we investigate models based on linear penalties as well as on quadratic penalties.

### 1.3 | Robust optimization

Robust optimization approaches are well-studied for intensity-modulated radiation therapy (IMRT) and intensity-modulated proton therapy (IMPT).<sup>36</sup> A common purpose of robust optimization modeling is to improve upon the traditional margin-based formulation of the planning target volume (PTV) to instead include uncertainty in the delineation from medical images, but it is also used to handle for example organ motion and setup uncertainties.

The data used for treatment planning is always to some extent uncertain. A starting point for robust optimization can be to model and estimate uncertainties in the form of scenarios, for example, from a probability distribution. Using the terminology from Unkelbach et al.,<sup>36</sup> classifications for robust approaches are (i) stochastic programming, which considers the average over all sampled scenarios, (ii) minimax optimization, which considers only the worst-case scenario, and (iii) minimax stochastic programming, which considers the worst-case of a number of probability distributions for the sampled scenarios; the approaches (i) and (ii) are special cases of (iii).

In HDR BT, there are two studies on robust optimization.<sup>37,38</sup> One study<sup>37</sup> considers uncertainty in the delineation of the target, based on a number of delineation scenarios, instead of the common practice to extend the target with a fixed margin. Uncertainties in the delineations of OARs are also studied. Another study<sup>38</sup> considers uncertainty in both catheter placement and in volume delineations. To our best knowledge, there are no IMBT studies using robust optimization.

## 1.4 | Purpose of our study

While previous studies have demonstrated the potential treatment benefits of IMBT, we focus on questions related to rotational uncertainty in the IMBT treatment delivery and the dosimetric effects from rotational errors. Robust optimization is a well-established way to take uncertainty into account in optimization models, and we apply robust versions of commonly used dose planning models to mitigate these dosimetric effects.

This uncertainty is due to the rotation of the shields during the treatment in IMBT and is not present in conventional HDR BT. Other types of uncertainties in HDR BT have been analyzed previously and published in a review article by GEC-ESTRO and AAPM,<sup>39</sup> and in the above-mentioned robust optimization studies.

## 2 | MATERIALS AND METHODS

Our study is based on the existing delivery prototype for prostate IMBT with platinum shields, developed by Famulari et al.,<sup>15</sup> in which the isotope <sup>169</sup>Yb, with a mean energy of 93 keV, is used. All catheters are identical and interior shields are rotating in steps of 22.5°, which gives 16 angles, and thus 16 dwell time variables for each dwell position. The shields rotate simultaneously in the catheters, and, therefore, the shield angles are the same in all catheters at each time during delivery. Illustrations of the prototype and the shield design are presented in Famulari et al.<sup>15</sup>

## 2.1 | Monte Carlo simulations

The Geant4<sup>40,41</sup> based treatment planning system RapidBrachyMCTPS<sup>42,43</sup> has been used for the study, including the Monte Carlo-based dose calculations, the implementation of the optimization models, and the evaluation of the resulting dose plans. Ultrasound was used for the medical imaging, and the patient geometries were approximated to be water equivalent with unit mass density. The high-Z material of the shields, being the most important nonwater heterogeneity, was, however, taken into account in the dose calculations, because the shields are in place in the catheters during the delivery. The number of photon histories for the model-based calculations of each combination of dwell position and shield angle was set to  $10^7$ , in order to achieve statistical uncertainties of less than 1% at the 40% and the 100% isodose levels, which are relevant for OAR and target doses. Dose points representing voxels of size 3 and 1 mm<sup>3</sup> are used for the optimization models and dose plan evaluations, respectively. Details about the Monte Carlo simulations, according to recommendations from the AAPM task group 268 (TG-268),<sup>44</sup> can be found in Appendix A, Table A1.

## 2.2 | Experimental design

We consider a nominal scenario in which there are no errors in shield angles, and two additional scenarios in which the shields have systematic rotational errors of  $\pm 10^\circ$ . It is furthermore assumed that the rotational error is the same in all catheters. This assumption and the estimate of the rotational errors are based on Famulari et al.<sup>15</sup> The errors are chosen to be outcomes with small probabilities to occur; hence, they can be regarded as worst-case outcomes with respect to rotational uncertainty. To test the proposed optimization models, we, however, also investigate scenarios with errors of  $\pm 20^\circ$ .

To assess how sensitive the dose distribution is with respect to rotational errors, we first obtain dwell times from the standard model and evaluate this dose plan in the scenarios with rotational errors. Of particular interest is the worst-case outcome with respect to DIs. In a second step, we take all three scenarios into account in a robust model.

## 2.3 | Patient cohort

We have used a data set of six patients treated for prostate cancer. The data set comes from two clinics, referred to as A and B, which use the same treatment protocol, which is 50 Gy external beam radiotherapy and two fractions of 10 Gy <sup>192</sup>Ir HDR BT boost. The strategies of these clinics regarding the number of inserted catheters and their placements are, however, somewhat

**TABLE 1** Characteristics of the patients in the data set. There is one dwell time variable for each combination of dwell position and shield angle.

Patient	Volumes (cc)				Number of	
	PTV	CTV	Rectum	Urethra	Catheters	Dwell time var.
A1	34.7	23.3	3.2	0.25	14	1424
A2	32.2	20.5	3.3	0.25	14	1216
A3	39.5	26.1	3.7	0.28	15	1520
B1	35.5	23.8	3.3	0.70	20	2560
B2	43.9	30.1	3.9	0.84	17	2448
B3	41.9	29.4	3.3	0.70	22	2816

different. At clinic B, more catheters are inserted than at clinic A, on average 20 and 14, respectively, and hence there are more possible dwell positions at clinic B. For both clinics, the clinical target volume (CTV), the PTV, the urethra, and the rectum were outlined on the ultrasound images.

Table 1 presents characteristics of the patient data set and Figure 1 shows examples of contoured structures for two patients. The number of Monte Carlo simulated dose distributions per patient is the number of scenarios multiplied with the numbers of dwell positions and shield angles. For our patient data set, the number of simulations varied between 3648 and 8448.

## 2.4 | Mathematical model

We propose a robust extension of the LPM, referred to as the robust linear penalty model (LPM-R); the model is presented by equations (1a)–(1h) with the notation given in Table 2. Clearly, with only one scenario, LPM-R reduces to the LPM. A robust extension of a QPM is presented in Appendix B.

$$\min z^w + \frac{1}{|R|} \sum_{r \in R} z^r \quad (1a)$$

subject to

$$\sum_{s \in S} w_s^l \sum_{i \in P_s} x_i^{rl} + \sum_{s \in S} w_s^u \sum_{i \in P_s} x_i^{ru} \leq z^r \quad r \in R \quad (1b)$$

$$z^r \leq z^w \quad r \in R \quad (1c)$$

$$\sum_{j \in J} d_{ij}^r t_j \geq L^s - x_i^{rl} \quad i \in P_s, s \in S, r \in R \quad (1d)$$

$$\sum_{j \in J} d_{ij}^r t_j \leq U^s + x_i^{ru} \quad i \in P_s, s \in S, r \in R \quad (1e)$$

$$x_i^{rl} \geq 0 \quad i \in P_s, s \in S, r \in R \quad (1f)$$

$$x_i^{ru} \geq 0 \quad i \in P_s, s \in S, r \in R \quad (1g)$$

**TABLE 2** Indices, sets, parameters, and variables in the optimization model

Indices	
$i$	Index for a dose point
$j$	Index for a combination of a dwell position and shield angle
$s$	Index for a structure
$r$	Index for a scenario
Sets	
$S$	Set of structures, including PTV, CTV, rectum, and urethra
$P_s$	Set of dose points in structure $s \in S$
$J$	Set of dwell position and shield angle combinations
$R$	Set of scenarios
Parameters	
$d_{ij}^r$	Dose-rate contribution from dwell position and shield angle $j \in J$ to dose point $i \in U_{s \in S} P_s$ in scenario $r \in R$
$L^s$	Prescription dose or lower dose bound for structure $s \in S$
$U^s$	Upper dose bound for structure $s \in S$
$w_s^l$	Non-negative penalty for dose being too low in structure $s \in S$
$w_s^u$	Non-negative penalty for dose being too high in structure $s \in S$
Variables	
$t_j$	Dwell time for dwell position and shield angle $j \in J$
$x_i^{rl}$	Penalty variable for dose being too low at dose point $i \in P_s, s \in S$ , in scenario $r \in R$
$x_i^{ru}$	Penalty variable for dose being too high at dose point $i \in P_s, s \in S$ , in scenario $r \in R$
$z^r$	Objective function value for scenario $r \in R$
$z^w$	Objective function value for the scenario with the worst-case outcome

$$t_j \geq 0 \quad j \in J \quad (1h)$$

This model belongs to the class of minimax stochastic programming. The objective function is a weighted sum of the penalty for the scenario with the worst-case outcome and the average penalty for the scenarios. The weight on the worst-case scenario is significantly higher than that of the other scenarios; with three scenarios, the weight becomes four times higher. Using the terminology of probability distributions, this model aims at minimizing the worst-case probability distribution among the following three distributions (i) (4/6, 1/6, 1/6) (ii) (1/6, 4/6, 1/6), (iii) (1/6, 1/6, 4/6), where the probabilities correspond to the three scenarios with errors of  $0^\circ$ ,  $+10^\circ$ , and  $-10^\circ$ , respectively (or 0, +20, -20).

Constraints (1b) ensure that the penalty variable for each scenario takes the correct value, and constraints (1c) ensure that the penalty variable for the

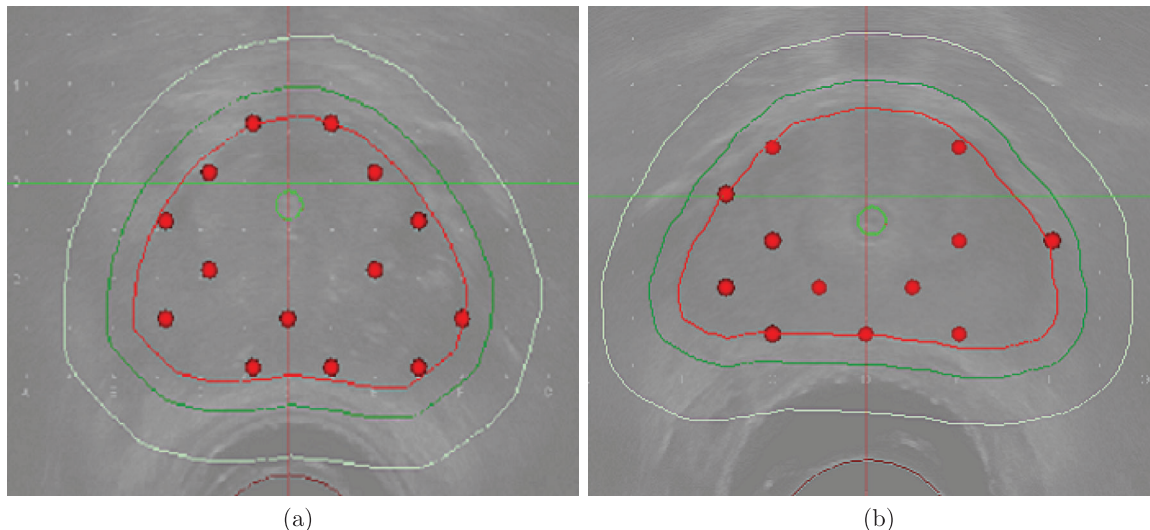


**FIGURE 1** Contours for two patients. The urethra is the light green contour in the center, the CTV, the PTV, and the normal tissue are the red, dark green, and light green contours, respectively, from inside to outside. The rectum is the brown contour at the bottom and the filled red circles correspond to dwell positions.

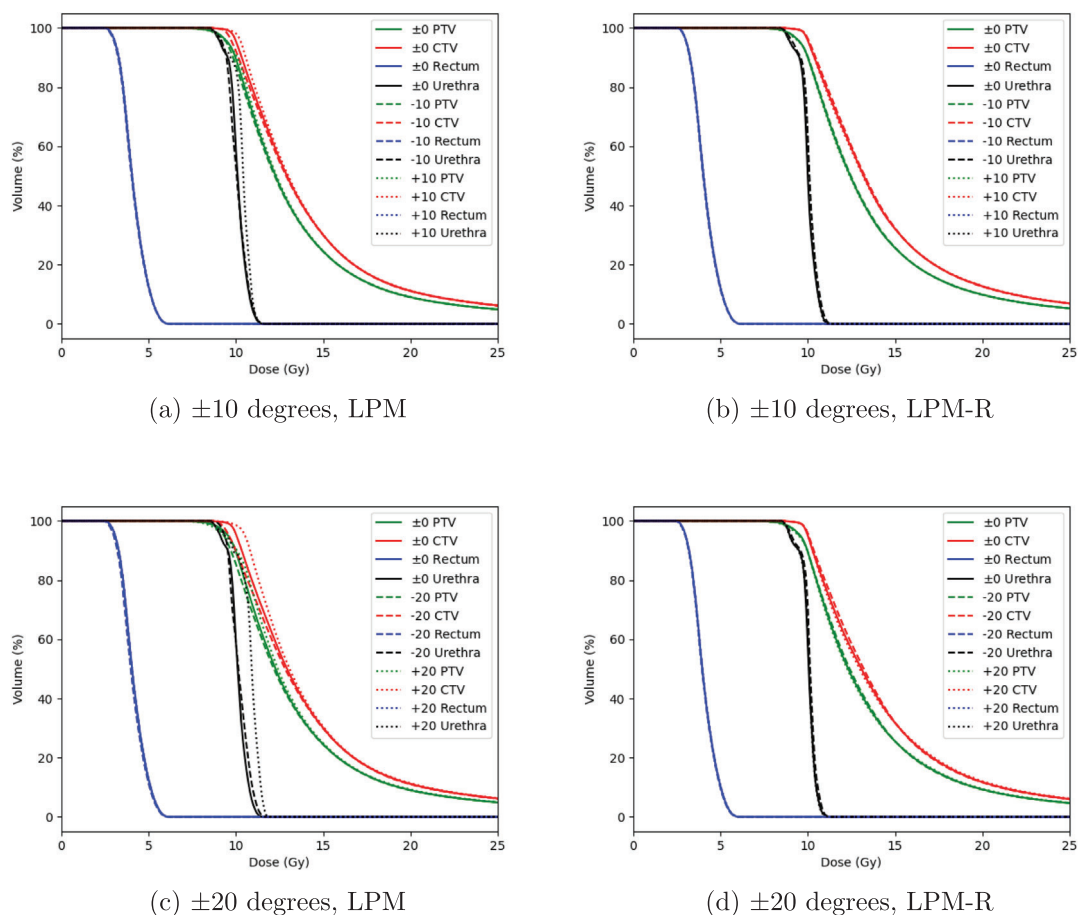


**FIGURE 2** DVHs for patient A1 for rotational errors of  $\pm 10^\circ$  and  $\pm 20^\circ$ . Results to the left are obtained from the LPM and results to the right are obtained from the LPM-R. The curves are, from left to right, for rectum, urethra, PTV, and CTV.

**TABLE 3** Dosimetric index values for PTV and OARs for clinic A for 10° and 20° errors. Results for the nominal scenario are presented as absolute values, while results for the other scenarios are presented as relative values compared to the corresponding nominal scenario. The unit for  $D_{90}$ ,  $D_{98}$ ,  $D_{0.1cc}$ , and  $D_{1cc}$  is Gy and the unit for  $V_{100}$ ,  $V_{150}$ , and  $V_{200}$  is percent.

Pat.	Model	Scenario	PTV					Rectum		Urethra
			$D_{90}$	$D_{98}$	$V_{100}$	$V_{150}$	$V_{200}$	$D_{0.1cc}$	$D_{1cc}$	$D_{0.1cc}$
A1	LPM	0	10.0	9.0	89.5	24.3	9.0	5.5	4.4	10.2
A1	LPM	+10	1.01	0.99	1.02	1.00	1.01	1.00	1.00	1.03
A1	LPM	-10	0.99	1.00	0.97	1.00	0.99	1.00	0.99	1.00
A1	LPM	+20	1.03	0.99	1.03	1.02	1.04	0.99	1.00	1.08
A1	LPM	-20	0.97	0.97	0.95	1.00	0.99	0.99	0.99	1.00
A1	LPM-R	0	10.0	9.0	89.5	25.4	9.8	5.5	4.4	10.1
A1	LPM-R	+10	1.00	0.99	1.00	1.00	1.01	1.00	1.00	1.01
A1	LPM-R	-10	1.00	1.00	1.00	1.00	0.99	1.00	0.99	1.01
A1	LPM-R	0	10.0	9.0	89.5	25.5	9.3	5.4	4.3	10.1
A1	LPM-R	+20	1.00	0.99	1.00	1.00	1.05	1.00	1.00	1.00
A1	LPM-R	-20	1.00	0.99	1.00	1.01	0.98	0.99	1.00	1.01
A2	LPM	0	10.0	8.7	90.1	26.0	10.1	5.3	4.3	10.6
A2	LPM	+10	0.99	0.99	0.99	1.04	1.01	1.07	1.06	1.00
A2	LPM	-10	1.00	1.00	0.99	0.96	0.99	0.96	0.96	1.03
A2	LPM	+20	0.99	0.99	0.98	1.08	1.03	1.18	1.14	1.04
A2	LPM	-20	0.96	0.93	0.95	0.95	0.98	0.93	0.94	1.07
A2	LPM-R	0	10.0	8.6	89.7	24.1	9.5	5.4	4.4	10.4
A2	LPM-R	+10	1.00	0.99	1.00	1.02	1.01	1.03	1.03	1.01
A2	LPM-R	-10	1.00	1.00	1.00	0.98	0.99	0.98	0.98	1.02
A2	LPM-R	0	10.0	8.8	90.0	23.5	9.1	5.5	4.6	10.3
A2	LPM-R	+20	1.00	1.00	1.00	1.06	1.04	1.04	1.03	1.00
A2	LPM-R	-20	1.00	0.98	1.00	0.95	0.96	1.01	1.01	1.00
A3	LPM	0	10.0	9.2	90.0	27.8	11.6	4.6	3.8	9.8
A3	LPM	+10	1.00	0.99	1.00	1.01	1.02	1.00	1.00	1.04
A3	LPM	-10	1.00	0.99	1.00	1.00	0.99	1.00	1.00	1.02
A3	LPM	+20	1.00	0.98	1.00	1.01	1.03	1.02	1.02	1.11
A3	LPM	-20	0.99	0.96	0.99	1.01	0.99	1.00	1.00	1.10
A3	LPM-R	0	10.0	9.0	90.0	28.2	11.3	4.7	3.9	9.9
A3	LPM-R	+10	1.00	0.99	1.00	0.99	1.00	1.00	1.00	1.03
A3	LPM-R	-10	1.00	0.99	1.00	1.01	1.00	1.00	1.00	1.01
A3	LPM-R	0	10.0	9.3	90.0	26.7	10.6	4.8	4.1	9.9
A3	LPM-R	+20	1.00	0.98	1.01	0.97	0.98	1.00	1.00	1.01
A3	LPM-R	-20	1.00	0.99	1.01	1.02	1.01	1.01	1.00	1.00

worst-case scenario takes the correct value. Constraints (1d)–(1g) are definitional constraints for the lower and upper linear penalty variables. Even though there is only a single dwell time variable for each combination of dwell position and shield angle, its contribution to the received dose at a dose point depends on the scenario considered. Therefore, there is a set of penalty variables for each scenario.

To solve the optimization models, Gurobi version 8.<sup>145</sup> (Gurobi Optimization, Inc., Houston, USA) was used.

### 3 | RESULTS

Results for DIs obtained from LPM and LPM-R for the six patients are presented in Tables 3 and 4, for errors of 10° and 20°. For all presented results, we have normalized the  $D_{90}^{PTV}$  for the nominal scenario to 10 Gy, which is the prescription dose, to get comparable results between LPM and LPM-R. Throughout this section, we primarily consider the difference between the nominal and the worst-case scenario.

**TABLE 4** Dosimetric index values for PTV and OARs for clinic B for 10° and 20° errors. The presentation is the same as in Table 3.

Pat.	Model	Scenario	PTV					Rectum		Urethra
			$D_{90}$	$D_{98}$	$V_{100}$	$V_{150}$	$V_{200}$	$D_{0.1cc}$	$D_{1cc}$	$D_{0.1cc}$
B1	LPM	0	10.0	9.0	90.1	22.0	9.0	4.6	3.8	9.4
B1	LPM	+10	1.00	1.00	0.99	0.99	1.00	1.02	1.01	1.03
B1	LPM	-10	1.00	1.00	1.01	1.02	1.01	1.03	1.01	1.04
B1	LPM	+20	0.99	0.99	0.98	0.99	1.00	1.06	1.05	1.13
B1	LPM	-20	1.00	0.99	1.00	1.04	1.03	1.09	1.06	1.14
B1	LPM-R	0	10.0	9.0	90.1	23.6	9.7	4.5	3.8	9.3
B1	LPM-R	+10	1.01	1.01	1.01	1.00	1.00	1.01	1.02	1.03
B1	LPM-R	-10	1.00	1.00	1.00	1.00	1.00	1.03	1.01	1.02
B1	LPM-R	0	10.0	9.2	90.1	20.5	7.8	4.4	3.6	9.6
B1	LPM-R	+20	1.01	1.01	1.02	0.99	1.00	1.06	1.05	1.02
B1	LPM-R	-20	1.01	1.01	1.01	1.06	1.04	1.04	1.02	1.02
B2	LPM	0	10.0	9.0	90.0	23.4	9.8	4.7	3.9	9.5
B2	LPM	+10	1.01	1.00	1.02	1.01	1.00	1.00	0.99	1.05
B2	LPM	-10	1.00	1.00	1.00	0.98	0.99	1.06	1.03	1.03
B2	LPM	+20	1.03	0.98	1.03	1.02	1.00	1.03	1.01	1.17
B2	LPM	-20	1.00	0.98	1.00	0.96	0.97	1.15	1.09	1.14
B2	LPM-R	0	10.0	9.0	90.0	26.6	10.2	4.7	3.9	9.3
B2	LPM-R	+10	1.01	1.02	1.01	1.01	1.00	1.02	1.01	1.03
B2	LPM-R	-10	1.00	1.01	1.00	0.99	0.99	1.03	1.01	1.03
B2	LPM-R	0	10.0	9.2	90.0	21.4	8.6	4.6	3.7	9.7
B2	LPM-R	+20	1.01	1.00	1.01	1.03	1.01	1.05	1.05	1.01
B2	LPM-R	-20	1.00	0.99	1.01	1.02	1.00	1.06	1.06	1.01
B3	LPM	0	10.0	9.3	90.1	19.9	8.6	4.7	3.7	9.8
B3	LPM	+10	0.99	0.99	0.98	1.01	1.00	1.01	1.00	1.00
B3	LPM	-10	1.00	1.00	1.01	1.00	1.01	1.04	1.04	1.02
B3	LPM	+20	0.99	0.97	0.97	1.02	1.01	1.05	1.04	1.05
B3	LPM	-20	1.00	0.98	1.00	1.02	1.02	1.13	1.11	1.09
B3	LPM-R	0	10.0	9.2	90.0	18.9	7.7	4.7	3.7	9.7
B3	LPM-R	+10	1.00	1.00	1.00	1.01	1.00	1.01	1.01	1.01
B3	LPM-R	-10	1.00	1.00	1.00	1.00	1.01	1.02	1.02	1.00
B3	LPM-R	0	10.0	9.2	90.0	19.0	7.8	4.6	3.6	9.6
B3	LPM-R	+20	1.00	1.01	0.99	1.00	1.00	1.03	1.05	1.01
B3	LPM-R	-20	1.00	1.00	0.99	1.06	1.04	1.02	1.05	1.02

First, for errors of 10°, the deviations are most notable for the OARs. The average increase in  $D_{0.1cc}^{urethra}$  is 3.5 and 2.2% for the standard model LPM and the robust model LPM-R, respectively, and the average increase in  $D_{0.1cc}^{rectum}$  is 3.3 and 1.7% for the standard model LPM and the robust model LPM-R, respectively. For LPM, the largest increases for the worst-case scenario for  $D_{0.1cc}^{urethra}$  and  $D_{0.1cc}^{rectum}$  are 5 and 7%, respectively, while corresponding numbers for LPM-R are 3 and 3%, respectively.

Doses to the PTV are generally stable for both LPM and LPM-R. However, for patient A1,  $V_{100}^{PTV}$  is reduced with 3 percentage points with LPM while the largest

decrease of  $V_{100}^{PTV}$  with LPM-R is 0.4 percentage points (patient A2), compared with the value of the nominal LPM scenario.

The dose to the CTV changes similarly as the dose to the PTV, and the range of DI values for the six patients is smaller for the robust model than for the standard model. For  $V_{100}^{CTV}$ , the range is 92.0–98.8% and 95.3–98.7% for the worst scenarios for LPM and LPM-R, respectively. The values for  $D_{90}^{CTV}$  are in the range 10.1–10.8 and 10.3–10.7 Gy for the worst-case scenarios for LPM and LPM-R, respectively.

Second, for errors of 20°, the pattern for OARs is similar, although there are larger deviations with LPM than

**TABLE 5** Relations between number of active dwell positions, longest dwell time, and the total dwell times, between LPM and LPM-R, calculated as LPM-R/LPM (%). For example, a value of 125% means that the number of active dwell positions in the dose plan obtained from LPM-R is 25% higher than in the plan from LPM.

Patient	Scenario	Active dwells	Longest dwell	Total time
A1	±10	125%	110%	101%
A2	±10	111%	114%	100%
A3	±10	123%	66%	99%
B1	±10	122%	133%	105%
B2	±10	106%	77%	101%
B3	±10	119%	81%	100%
A1	±20	143%	89%	99%
A2	±20	134%	85%	100%
A3	±20	125%	54%	97%
B1	±20	150%	85%	101%
B2	±20	141%	99%	98%
B3	±20	129%	121%	103%

for the case with 10° errors. The deviations for OARs with LPM-R are, however, closer to the ones from the 10° errors, although a bit higher for the rectum. For the PTV coverage, there are larger deviations for LPM with 20° errors than for the case with 10° errors, while the PTV coverage is stable for LPM-R also for this larger error.

Figure 2 compares scenarios with rotational errors of 10° and 20°, for patient A1. From the DVHs, it is clear that there are larger deviations when using LPM with 20° errors, as illustrated in Figure 2c, than for 10° errors shown in Figure 2a, in particular for the urethra. However, the DVHs are similar when using LPM-R with 10° and 20° errors as presented in Figures 2b, and 2d, respectively, which shows that the robust model is capable of handling rotational errors larger than 10°. Hence, if there are larger rotational errors than expected, the robust model will be even more useful.

As presented in Tables 3 and 4 no clear relationship between the number of catheters and the robustness of the nominal scenario can be observed. One systematic difference in the results for the patients from the two clinics is that  $V_{150}^{PTV}$  and  $V_{200}^{PTV}$  are higher for patients from clinic A, which can be an effect of fewer catheters being inserted.

Table 5 shows a comparison of the dwell time statistics for LPM and LPM-R, with 10° errors; a value above 100% means an increase for LPM-R. There is a systematic trend of more active dwell positions in dose plans obtained from LPM-R than with LPM, on average 18% more dwell positions are active with LPM-R. The differences in total dwell times for the two models are small, but the average dwell time is shorter for LPM-R, due to its higher number of nonzero dwell times.

Finally, we also tested extensions of the LPM and LPM-R with both linear and quadratic penalties, instead of only linear penalties. These models are referred to as the QPM and the QPM-R, respectively; see Appendix B for the mathematical models. Results for patients A1 and B1 are given in Table 6.

## 4 | DISCUSSION AND FUTURE RESEARCH

The results presented in Section 3, for example, in Table 3, show that for the dose plan obtained from the LPM, the DIs for both target coverage and OARs are impaired in the worst-case scenario. This possibly detrimental effect was shown to be effectively mitigated by the robust approach LPM-R. Hence, the robust extension of the LPM provides a safeguard against rotational uncertainty. Although the patient material is rather limited, results for OAR doses regarding the deviations obtained from LPM and LPM-R are consistent between the patients. For all patients and evaluation criteria for OARs, the deviation of the worst-case scenario is smaller with LPM-R than with LPM. The benefits in DIs when replacing LPM with LPM-R may not be of clinical significance, but as the nominal plans from LPM-R are slightly better than those from the LPM, there is no trade-off in terms of dose plan quality. From a mathematical optimization point of view this seems to be unexpected. However, as can be expected, the objective function value for the nominal scenario is higher in LPM-R than in LPM, but the higher objective value is not reflected by the DIs. This can be explained with the previously observed weak correlation between the objective value of the LPM and the DIs.<sup>19,24</sup>

The drawback of using the LPM-R is that more dose calculations are needed (three times more due to the three scenarios), resulting in considerably longer computing times for such a dose planning model. In this concept study, we have not worked on improving computing times, and we expect that they can be significantly shortened, for example, by using deep learning for the model-based dose calculations.<sup>46</sup>

In this study, we consider only systematic rotational errors, that is, rotational errors that are common for all dwell positions. There can also be random rotational errors for individual dwell positions. However, we consider the effects from these random components to be considerably smaller than the systematic ones, and hence we only studied the latter.

Our results are based on a specific delivery prototype.<sup>15</sup> The same modeling approach can be applied to other delivery techniques, although the modeling of scenarios and worst-case errors might differ. We expect that the robust optimization approach works well also for other suggested techniques for IMBT.

**TABLE 6** Dosimetric index values for PTV and OARs obtained from QPM and QPM-R, in comparison with LPM and LPM-R for 10° errors. The presentation is the same as in Table 3.

Patient	Model	Scenario	PTV					Rectum		Urethra
			$D_{90}$	$D_{98}$	$V_{100}$	$V_{150}$	$V_{200}$	$D_{0.1cc}$	$D_{1cc}$	$D_{0.1cc}$
A1	LPM	0	10.0	9.0	89.5	24.3	9.0	5.5	4.4	10.2
A1	LPM	+10	1.01	0.99	1.02	1.00	1.01	1.00	1.00	1.03
A1	LPM	-10	0.99	1.00	0.97	1.00	0.99	1.00	0.99	1.00
A1	LPM-R	0	10.0	9.0	89.5	25.4	9.8	5.5	4.4	10.1
A1	LPM-R	+10	1.00	0.99	1.00	1.00	1.01	1.00	1.00	1.01
A1	LPM-R	-10	1.00	1.00	1.00	1.00	0.99	1.00	0.99	1.01
A1	QPM	0	10.0	8.9	89.3	18.9	7.2	5.3	4.3	10.2
A1	QPM	+10	1.01	0.99	1.01	1.02	1.01	1.01	1.01	1.03
A1	QPM	-10	0.98	1.00	0.97	0.99	0.99	1.00	0.99	0.99
A1	QPM-R	0	10.0	9.0	89.5	19.1	7.0	5.3	4.2	10.1
A1	QPM-R	+10	1.00	0.99	0.99	1.01	1.00	1.01	1.01	1.00
A1	QPM-R	-10	1.00	1.00	1.00	1.00	1.00	0.99	0.99	1.01
B1	LPM	0	10.0	9.1	90.0	23.3	8.2	4.5	3.7	9.4
B1	LPM	+10	1.00	0.99	1.00	0.99	1.00	1.02	1.01	1.03
B1	LPM	-10	1.00	0.99	1.01	1.02	1.02	1.03	1.01	1.03
B1	LPM-R	0	10.0	9.1	90.0	24.6	8.4	4.4	3.7	9.3
B1	LPM-R	+10	1.01	1.01	1.01	1.00	1.00	1.01	1.02	1.03
B1	LPM-R	-10	1.00	1.00	1.00	1.01	0.99	1.02	1.01	1.02
B1	QPM	0	10.0	9.0	90.0	26.2	7.7	4.5	3.8	8.9
B1	QPM	+10	1.00	1.00	1.00	1.00	1.00	1.02	1.01	1.03
B1	QPM	-10	1.00	1.01	1.01	1.02	1.01	1.04	1.02	1.04
B1	QPM-R	0	10.0	9.0	90.0	28.8	7.9	4.6	3.9	8.8
B1	QPM-R	+10	1.00	1.02	1.00	1.00	0.99	1.02	1.02	1.03
B1	QPM-R	-10	1.01	1.02	1.01	1.01	1.01	1.03	1.01	1.04

In terms of robustness, the improvements gained when replacing QPM with QPM-R are similar to those gained when replacing LPM with LPM-R. Thus, the robust modeling approach, including both the average penalty and the worst-case penalty, does not appear to rely on the specific choice of dose planning model to be able to produce robust dose plans. The computing times are significantly longer with QPM-R, but with a tailored implementation, we expect computing times to be acceptable from a clinical perspective.

The dose distributions used in this study were simulated based on ultrasound images. The geometries on these images are smaller than the actual patient geometries and the total dose is hence somewhat underestimated due to reduced contribution of dose from scattered photons. The dose reduction due to the shields in the phantoms used are, however, accurately estimated. A reason for not extending the ultrasound geometries is that a larger phantom increases the computational complexity, both regarding the model-based calculations for each combination of dwell position and shield angle, and the memory requirements of the

RapidBrachyMCTPS. We have further compared the dose distributions used in this study with those obtained when extending the ultrasound images with a surrounding water phantom. Results for DIs from the latter dose distributions were very close to the ones included in this study; we compared the outcomes from the two dose distributions for the different scenarios and the differences for dose-at-volume criteria between the nominal scenario and the worst-case scenario were generally within 0.1 Gy.

We have in this work conducted the dose planning based on a catheter placement, which was used clinically for the conventional  $^{192}\text{Ir}$  HDR BT treatment. In order to spare the urethra, the catheters were thus not placed close to the urethra. It is, therefore, likely that there is room for improvements in the dose planning by also including the catheter placement in the model. By allowing catheters to be placed closer to the urethra, we could achieve better target coverage while also taking advantage of the shields to spare the urethra. However, such a dose plan may be less robust with respect to rotational shield errors, and the potential of using robust

optimization for the combined catheter placement and dose planning problem could, therefore, be higher than what is shown in this study. Such a study on catheter placement would benefit from faster dose calculations, for example using deep learning for the model-based dose calculations.

We have tried two dose planning models, LPM and QPM. It could be of interest to consider also a dose–volume model, for example, with the aim to minimize  $D_{0.1cc}^{urethra}$  in the worst-case scenario. A robust approach based on a dose–volume model is very challenging computationally, but the results in terms of DIs can probably be improved.

An extension of this study would be to consider a larger number of scenarios, for example with rotational errors, which are specific for each catheter or even for each dwell position. This might be relevant for another delivery system. It is also possible to include scenarios with translational errors in the source positioning. The proposed robust models can be used also in such a study.

A straightforward continuation of this work would be to apply the proposed robust models to other treatment sites, such as, for example, cervical cancer.

## 5 | CONCLUSIONS

The proposed robust optimization model for dose planning of IMBT improves the results for the worst-case scenario, without impairing the outcome for the nominal scenario in terms of dose plan quality. Hence, the robust approach can be used as a safeguard against rotational uncertainty, without sacrificing the expected outcome of the treatment.

## ACKNOWLEDGMENTS

This research was enabled in part by support provided by Cedar computer cluster (WestGrid, <https://www.westgrid.ca>) and Compute Canada ([www.computecanada.ca](http://www.computecanada.ca)). Björn Morén, Torbjörn Larsson, and Åsa Carlsson Tedgren acknowledge funding from the Swedish Research Council, Grant No. VR-NT 2019-05416, Åsa Carlsson Tedgren acknowledges funding from the Swedish Cancer Society, Grants Nos. CAN 2017/1029 and Pj 211788, and Shirin A. Enger acknowledges funding from Canada Research Chairs program, Grant No. 252135 and CHRP, NSERC CIHR Grant No. 523394-18.

## CONFLICT OF INTEREST

The authors have no conflicts to disclose.

## DATA AVAILABILITY STATEMENT

The authors are not able to share the patient data used in this study.

## REFERENCES

- Ebert MA. Possibilities for intensity-modulated brachytherapy: technical limitations on the use of non-isotropic sources. *Phys Med Biol.* 2002;47:2495-2509.
- Shoemaker T, Vuong T, Glickman H, Kaifi S, Famulari G, Enger SA. Dosimetric considerations for yttrium-169, Selenium-75, and Iridium-192 radioisotopes in high-dose-rate endorectal brachytherapy. *Int J Radiat Oncol Biol Phys.* 2019;105:875-883.
- Dupere JM, Munro JJ, Medich DC. Intensity modulated high dose rate ocular brachytherapy using Se-75. *Brachytherapy.* 2021;20:1312-1322.
- Morcos M, Viswanathan AN, Enger SA. On the impact of absorbed dose specification, tissue heterogeneities, and applicator heterogeneities on Monte Carlo-based dosimetry of Ir-192, Se-75, and Yb-169 in conventional and intensity-modulated brachytherapy for the treatment of cervical cancer. *Med Phys.* 2021;48:2604-2613.
- Reynoso FJ, Munro JJ, Cho SH. Technical note: Monte Carlo calculations of the AAPM TG-43 brachytherapy dosimetry parameters for a new titaniumencapsulated Yb-169 source. *J Appl Clin Med Phys.* 2017;18:193-199.
- Das RK, Mishra V, Perera H, Meigooni AS, Williamson JF. A secondary air kerma strength standard for Yb-169 interstitial brachytherapy sources. *Phys Med Biol.* 1995;40:741-756.
- Mason DLD, Battista JJ, Barnett RB, Porter AT. Ytterbium-169: Calculated physical properties of a new radiation source for brachytherapy. *Med Phys.* 1992;19:695-703.
- Perera H, Williamson JF, Li Z, Mishra V, Meigooni AS. Dosimetric characteristics, air-kerma strength calibration and verification of Monte Carlo simulation for a new ytterbium-169 brachytherapy source. *Int J Radiat Oncol Biol Phys.* 1994;28:953-970.
- Enger SA, Fisher DR, Flynn RT. Gadolinium-153 as a brachytherapy isotope. *Phys Med Biol.* 2013;58:957-964.
- Famulari G, Urlich T, Armstrong A, Enger SA. Practical aspects of <sup>153</sup>Gd as a radioactive source for use in brachytherapy. *Appl Radiat Isot.* 2017;130:131-139.
- Yamada Y, Rogers L, Demanes DJ, et al. American Brachytherapy Society consensus guidelines for high-dose-rate prostate brachytherapy. *Brachytherapy.* 2012;11:20-32.
- Hoskin PJ, Colombo A, Henry A, et al. GEC/ESTRO recommendations on high dose rate afterloading brachytherapy for localised prostate cancer: an update. *Radiother Oncol.* 2013;107:325-332.
- Henry A, Pieters BR, André Siebert F, Hoskin P. GEC-ESTRO ACROP prostate brachytherapy guidelines. *Radiother Oncol.* 2022;167:244-251.
- Viswanathan AN, Beriwal S, De Los Santos JF, et al. American Brachytherapy Society consensus guidelines for locally advanced carcinoma of the cervix. Part II: high-dose-rate brachytherapy. *Brachytherapy.* 2012;11:47-52.
- Famulari G, Duclos M, Enger SA. A novel 169 Yb-based dynamic-shield intensity modulated brachytherapy delivery system for prostate cancer. *Med Phys.* 2020;47:859-868.
- Adams QE, Xu J, Breitbach EK, et al. Interstitial rotating shield brachytherapy for prostate cancer. *Med Phys.* 2014;41:51703.
- Morcos M, Antaki M, Viswanathan AN, Enger SA. A novel minimally invasive dynamic shield intensity modulated brachytherapy system for cervical cancer. *Med Phys.* 2021;48(1):71-79.
- Lessard E, Pouliot J. Inverse planning anatomy-based dose optimization for HDR-brachytherapy of the prostate using fast simulated annealing algorithm and dedicated objective function. *Med Phys.* 2001;28:773-779.
- Alterovitz R, Lessard E, Pouliot J, Hsu I-CJ, O'Brien JF, Goldberg K. Optimization of HDR brachytherapy dose distributions using linear programming with penalty costs. *Med Phys.* 2006;33:4012-4019.
- Holm Å, Larsson T, Carlsson Tedgren Å. Impact of using linear optimization models in dose planning for HDR brachytherapy. *Med Phys.* 2012;39:1021-1028.

21. Morén B, Larsson T, Carlsson Tedgren Å. Mathematical optimization of high dose-rate brachytherapy—derivation of a linear penalty model from a dose-volume model. *Phys Med Biol*. 2018;63:065011.
22. Beliën J, Colpaert J, De Boeck L, Demeulemeester E. A hybrid simulated annealing linear programming approach for treatment planning in HDR brachytherapy with dose volume constraints. In Proceedings of the 35th International Conference on Operational Research Applied to Health Services (ORAHS). 2009.
23. Siauw T, Cunha A, Atamtürk A, Hsu I-C, Pouliot J, Goldberg K. IPIP: a new approach to inverse planning for HDR brachytherapy by directly optimizing dosimetric indices. *Med Phys*. 2011;38:4045-4051.
24. Gorissen BL, den Hertog D, Hoffmann AL. Mixed integer programming improves comprehensibility and plan quality in inverse optimization of prostate HDR brachytherapy. *Phys Med Biol*. 2013;58:1041-1057.
25. Deist TM, Gorissen BL. High-dose-rate prostate brachytherapy inverse planning on dose-volume criteria by simulated annealing. *Phys Med Biol*. 2016;61:1155-1170.
26. Guthrie CV, Damato AL, Viswanathan AN, Hesser JW, Cormack RA. A fast multi-target inverse treatment planning strategy optimizing dosimetric measures for high-dose-rate (HDR) brachytherapy. *Med Phys*. 2017;44:4452-4462.
27. Morén B, Larsson T, Carlsson Tedgren Å. An extended dose-volume model in high dose-rate brachytherapy—using mean-tail-dose to reduce tumour underdosage. *Med Phys*. 2019;46:2556-2566.
28. Morén B, Larsson T, Carlsson Tedgren Å. A mathematical optimization model for spatial adjustments of dose distributions in high dose-rate brachytherapy. *Phys Med Biol*. 2019;64:225012.
29. Morén B, Larsson T, Carlsson Tedgren Å. Optimization in treatment planning of high dose-rate brachytherapy—review and analysis of mathematical models. *Med Phys*. 2021;48:2057-2082.
30. Callaghan CM, Adams Q, Flynn RT, Wu X, Xu W, Kim Y. Systematic review of intensity modulated brachytherapy (IMBT): static and dynamic techniques. *Int J Radiat Oncol Biol Phys*. 2019;105:206-221.
31. Shi C, Guo B, Cheng CY, Esquivel C, Eng T, Papanikolaou N. Three dimensional intensity modulated brachytherapy (IMBT): dosimetry algorithm and inverse treatment planning. *Med Phys*. 2010;37:3725-3737.
32. Webster MJ, Devic S, Vuong T, et al. Dynamic modulated brachytherapy (DMBT) for rectal cancer. *Med Phys*. 2013;40:011718.
33. Liu Y, Flynn RT, Kim Y, Wu X. Asymmetric dose-volume optimization with smoothness control for rotating-shield brachytherapy. *Med Phys*. 2014;41:111709.
34. Cho M, Wu X, Dadkhah H, et al. Fast dose optimization for rotating shield brachytherapy. *Med Phys*. 2017;44:5384-5392.
35. Antaki M, Deufel CL, Enger SA. Fast mixed integer optimization (FMIO) for high dose rate brachytherapy. *Phys Med Biol*. 2020;65:215005.
36. Unkelbach J, Alber M, Bangert M, et al. Robust radiotherapy planning. *Phys Med Biol*. 2018;63:22TR02.
37. Balvert M, Den Hertog D, Hoffmann AL. Robust optimization of dose-volume metrics for prostate HDR-brachytherapy incorporating target and oar volume delineation uncertainties. *INFORMS J. Comput*. 2019;31:100-114.
38. van der Meer MC, Bel A, Niatsetski Y, Alderliesten T, Pieters BR, Bosman PAN. Robust evolutionary bi-objective optimization for prostate cancer treatment with high-dose-rate brachytherapy. In: Bäck T, Preuss M, Deutz A, et al., eds. *Parallel Problem Solving from Nature—PPSN XVI*. Springer International Publishing; 2020:441-453.
39. Kirisits C, Rivard MJ, Baltas D, et al. Review of clinical brachytherapy uncertainties: analysis guidelines of GEC-ESTRO and the AAPM. *Radiother Oncol*. 2014;110:199-212.
40. Agostinelli S, Allison J, Amako K, et al. GEANT4—a simulation toolkit. *Nuclear Instrum Methods Phys Res, Section A: Accel, Spectrom, Detect Assoc Equip*. 2003;506:250-303.
41. Allison J, Amako K, Apostolakis J, et al. Geant4 developments and applications. *IEEE Trans Nucl Sci*. 2006;53:270-278.
42. Famulari G, Renaud MA, Poole CM, Evans MD, Seuntjens J, Enger SA. RapidBrachyMCTPS: A Monte Carlo-based treatment planning system for brachytherapy applications. *Phys Med Biol*. 2018;63:175007.
43. Glickman H, Antaki M, Deufel C, Enger SA. RapidBrachyMCTPS 2.0: a comprehensive and flexible Monte Carlo-based treatment planning system for brachytherapy applications. *arXiv preprint arXiv:2007.02902*. 2020.
44. Sechopoulos I, Rogers DW, Bazalova-Carter M, et al. RECORDS: improved Reporting of monte Carlo RaDiation transport Studies: Report of the AAPM Research Committee Task Group 268. *Med Phys*. 2018;45:e1-e5.
45. Gurobi Optimization LLC. *Gurobi Optimizer Reference Manual*. Gurobi Optimization, Inc; 2022.
46. Mao X, Pineau J, Keyes R, Enger SA. RapidBrachyDL: rapid radiation dose calculations in brachytherapy via deep learning. *Int J Radiat Oncol Biol Phys*. 2020;108:802-812.
47. Daskalov GM, Löffler E, Williamson JF. Monte Carlo-aided dosimetry of a new high dose-rate brachytherapy source. *Med Phys*. 1998;25:2200-2208.
48. Tulli JK. *Evaluated Nuclear Structure Data File, A Manual for Preparation of Data Sets*. Technical Report. 2001.
49. Cullen D, Hubbell J, Kissel L. EPDL97: *The Evaluated Photon Data Library*. 1997;6.
50. Perkins ST, Cullen DE, Seltzer SM, Laboratory LLN. Tables and Graphs of Electron-interaction Cross Sections from 10 eV to 100 GeV derived from the LLNL Evaluated Electron Data Library (EEDL), Z = 1–100. *Uclr-50400*. 1991;31:500.
51. Perkins ST, Cullen D, Chen MH, Rathkopf J, Scofield J, Hubbell JH. *Tables and Graphs of Atomic Subshell and Relaxation Data Derived from the LLNL Evaluated Atomic Data Library (EADL), Z = 1–100. UCRL-50400*. US Department of Energy, Office of Scientific and Technical Information; 1991.
52. Williamson JF. Monte Carlo evaluation of kerma at a point for photon transport problems. *Med Phys*. 1987;14:567-576.
53. Mann-Krzisnik D, Verhaegen F, Enger SA. The influence of tissue composition uncertainty on dose distributions in brachytherapy. *Radiother Oncol*. 2018;126:394-410.

**How to cite this article:** Morén B, Antaki M, Famulari G, et al. Dosimetric impact of a robust optimization approach to mitigate effects from rotational uncertainty in prostate intensity-modulated brachytherapy. *Med Phys*. 2023;50:1029–1043.  
<https://doi.org/10.1002/mp.16134>

## APPENDIX A: MONTE CARLO SIMULATION METHODS

See Table A1 for details about the Monte Carlo simulations, according to recommendations of TG-268.<sup>44</sup>

**TABLE A1** Monte Carlo simulation methods used to calculate the dose-rate contributions for this work. The simulation methods are based on the recommendations of TG-268.

Item name	Description
Code, version	RapidBrachyMCTPS, <sup>42,43</sup> Geant4 10.2 <sup>40,41</sup>
Validation	Previously validated <sup>42</sup>
Timing	Up to 10 min per dwell position on a 2 × Intel E5-2683 v4 Broadwell 2.1 GHz.
Geometry	Voxelized geometry (egsphant) extracted from DICOM ultrasound images and DICOM RT Structure Set files. Voxel size: for dwell time optimization a) 3 mm <sup>3</sup> and for final dose calculation b) 1 mm <sup>3</sup> .
Materials	Patient geometry estimated to be water equivalent with unit mass density, with the density of the shields taken into account.
Source description	MicroSelectron v2 source geometry. Explicit simulation of radioactive decay spectra from ENSDF. <sup>47,48</sup> Source positions and orientation imported from DICOM RT Plan files.
Cross sections	EPDL97, EEDL97, EADL97. <sup>49–51</sup>
Transport parameters	PENELOPE low-energy electromagnetic physics list with default transport parameters. Electron transport off. Production cut: 0.1 mm. <sup>42</sup>
Variance reduction technique	Tracklength estimator using mass-energy absorption coefficient library provided in RapidBrachyMCTPS. <sup>52,53</sup>
Scored quantities	Absorbed dose (collisional kerma approximation) scored to water. Voxel size: (a) 3 mm <sup>3</sup> and (b) 1 mm <sup>3</sup> .
#histories & statistical uncertainties	10 <sup>7</sup> decay events. Type A uncertainty for final dose calculation is 0.7% on the 100% isodose line and 0.9% on the 40% isodose line.
Statistical methods	History-by-history method.
Postprocessing	Dose to voxels converted into dose–volume parameters using RapidBrachyMCTPS.

## APPENDIX B: ROBUST QUADRATIC PENALTY MODEL

The robust linear-quadratic penalty model (QPM-R) is presented below. The notation is given in Tables 2 and B1.

$$\min z^w + \frac{1}{|R|} \sum_{r \in R} z^r \quad (\text{B1a})$$

subject to

$$\begin{aligned} \sum_{s \in S} \sum_{i \in P_s} \left( w_s^l x_i^{rl} + q_s^l (x_i^{rl})^2 + w_s^u x_i^{ru} + q_s^u (x_i^{ru})^2 \right) &\leq z^r & r \in R \\ z^r &\leq z^w & r \in R \\ \sum_{j \in J} d_{ij}^r t_j &\geq L^s - x_i^{rl} & i \in P_s, s \in S, r \in R \\ \sum_{j \in J} d_{ij}^r t_j &\leq U^s + x_i^{ru} & i \in P_s, s \in S, r \in R \\ x_i^{rl} &\geq 0 & i \in P_s, s \in S, r \in R \\ x_i^{ru} &\geq 0 & i \in P_s, s \in S, r \in R \\ t_j &\geq 0 & j \in J \end{aligned} \quad (\text{B1b})$$

The only difference to the model LPM-R is the first constraint, in which the penalty for each scenario is calculated. Here, the penalty is a weighted sum of linear and quadratic components. If the set  $R$  contains only the nominal scenario, we get the formulation QPM.

**TABLE B1** Parameters in the quadratic penalty model

Parameters	
$q_s^l$	Non-negative quadratic penalty for dose being too low in structure $s \in S$
$q_s^u$	Non-negative quadratic penalty for dose being too high in structure $s \in S$

**APPENDIX C: ADDITIONAL RESULTS**

Figures C1–C5 show DVHs for patients A2–A3 and B1–B3, for both LPM and LPM-R and for each of the three scenarios for 10° and 20° errors.

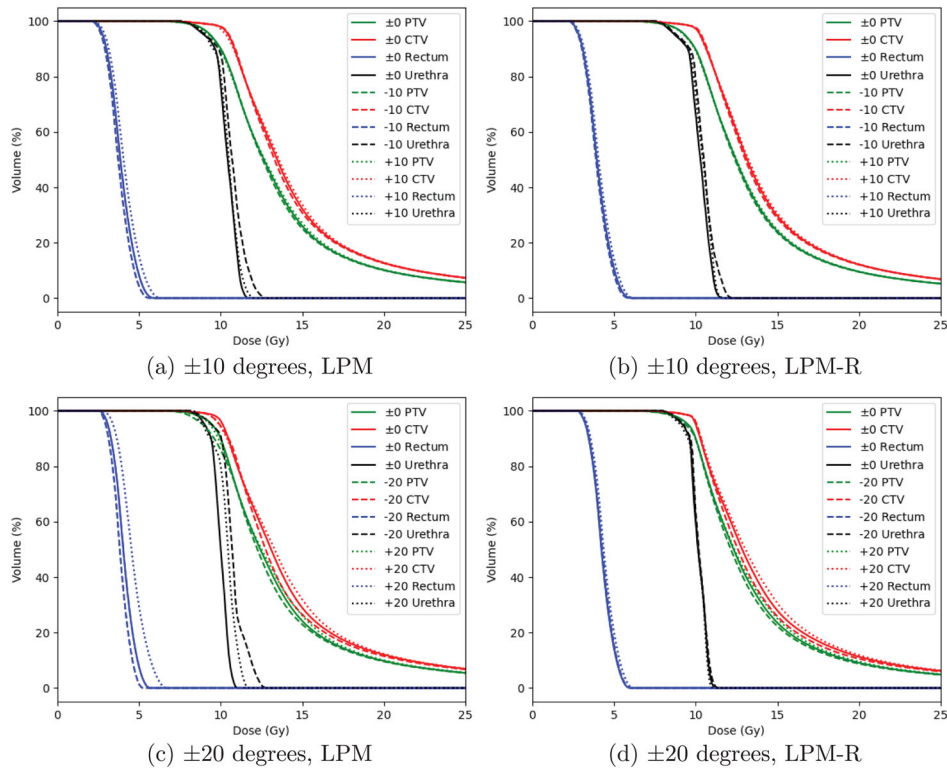


**FIGURE C1** DVHs for patient A2. The curves are, from left to right, for rectum, urethra, PTV, and CTV.

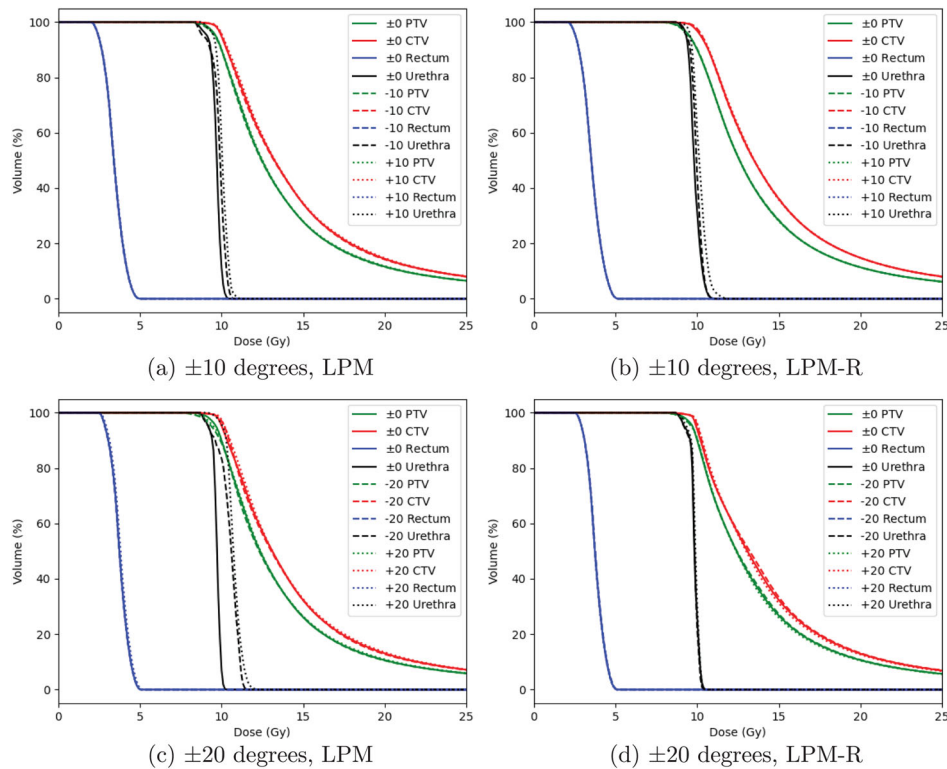


**FIGURE C2** DVHs for patient A3. The curves are, from left to right, for rectum, urethra, PTV, and CTV.

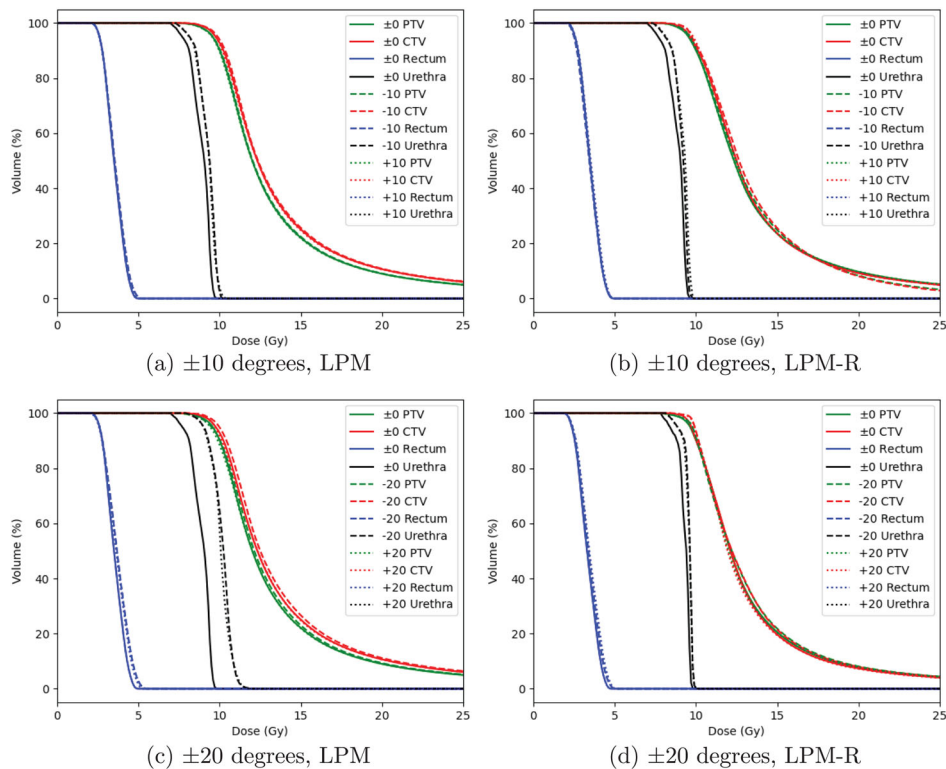


FIGURE C3 DVHs for patient B1. The curves are, from left to right, for rectum, urethra, PTV, and CTV.

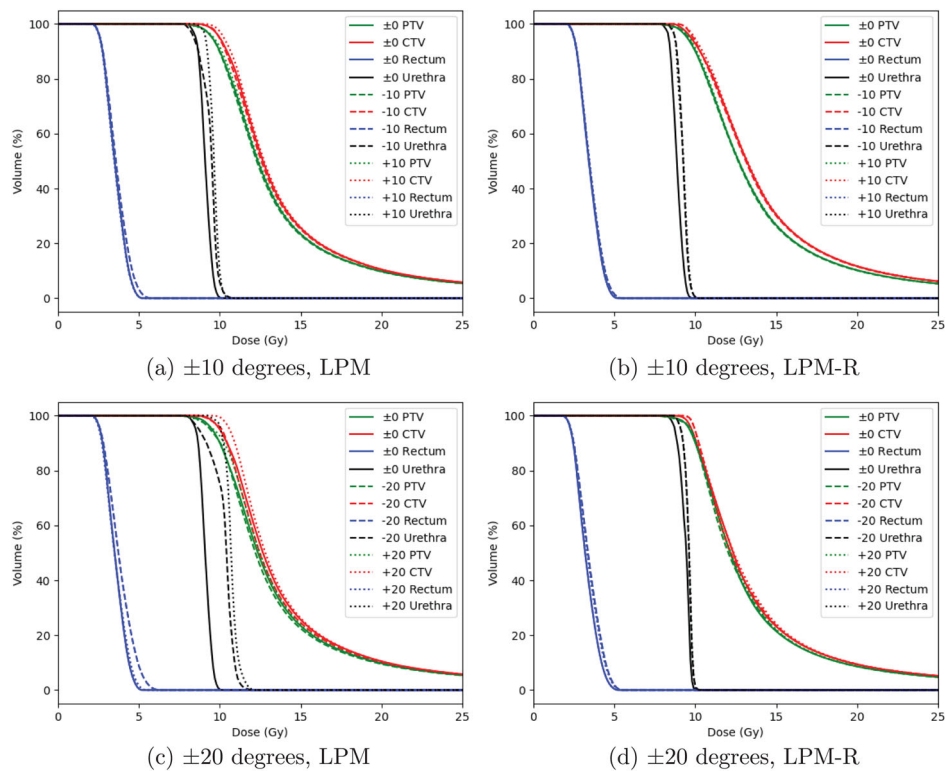
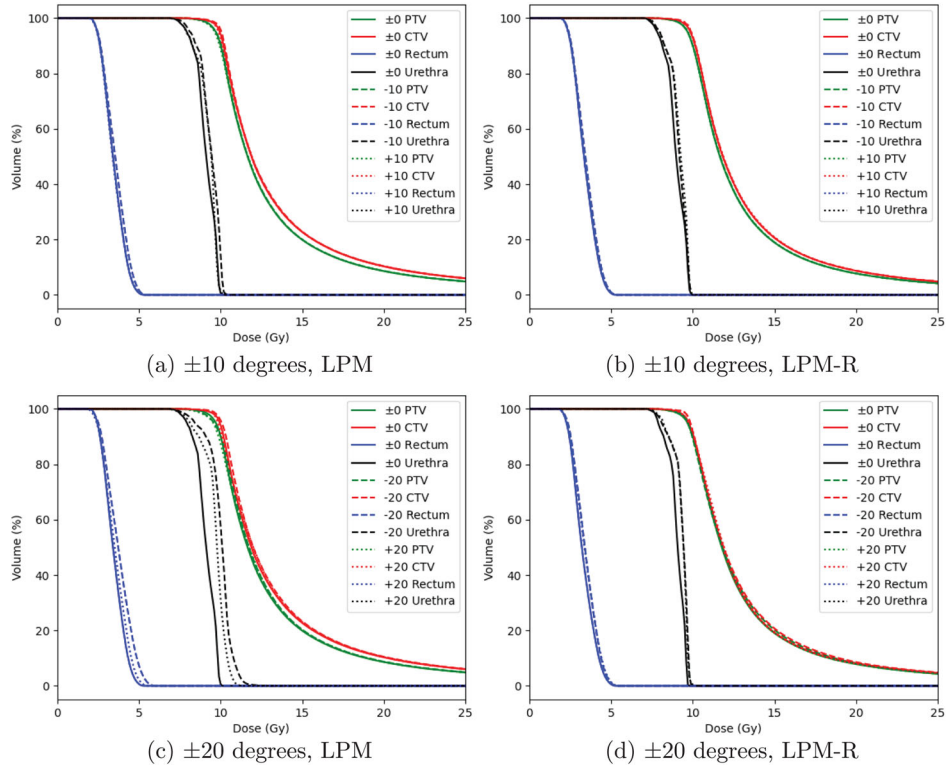


FIGURE C4 DVHs for patient B2. The curves are, from left to right, for rectum, urethra, PTV, and CTV.



**FIGURE C5** DVHs for patient B3. The curves are, from left to right, for rectum, urethra, PTV, and CTV.